

Chapter 2

Carbon Nanotube: Properties and Applications

Abstract This chapter presents the unique atomic structure and properties of carbon nanotube (CNT). The electronic band structure of carbon nanotube along with their small size and low dimension are responsible for their unique electrical, mechanical, and thermal properties. This chapter summarizes the electronic band structure of one-dimensional CNTs, various transport properties, and their real-world applications. Additionally, a brief about the production and purification of CNTs is also presented in this chapter.

Keywords Carbon nanotube (CNT) • Single-walled CNT (SWNT) • Double-walled CNT (DWNT) • Multi-walled CNT (MWNT) • Tight binding approximation • Chemical vapor deposition (CVD)

2.1 Introduction

A carbon atom can form various types of allotropes. In 3D structures, diamond and graphite are the allotropes of carbon. Carbon also forms low-dimensional (2D, 1D or 0D) allotropes collectively known as carbon nanomaterials. Examples of such nanomaterials are 1D carbon nanotubes (CNTs) and 0D fullerenes. In the list of carbon nanomaterials, graphene is known as 2D single layer of graphite. The sp^2 bonds in graphene is stronger than sp^3 bonds in diamond that makes graphene the strongest material (Sarkar et al. 2011). The lattice structure of graphene in real space consists of hexagonal arrangement of carbon atoms as shown in Fig. 2.1a. An isolated carbon atoms have four valence electrons in its $2s$, and $2p$ atomic orbitals. While forming into graphene, three atomic orbitals of the carbon atom, $2s$, $2p_x$, and $2p_y$, are hybridized into three sp^2 orbitals. These sp^2 orbitals are in the same plane while the remaining $2p_z$ is perpendicular to other orbitals as shown in Fig. 2.1b (Sarkar et al. 2011). The σ bonds between the adjacent carbon atoms are formed by the sp^2 hybridized orbitals, whereas the $2p_z$ orbitals form the π bonds that are out of the plane of graphene (Javey and Kong, 2009).

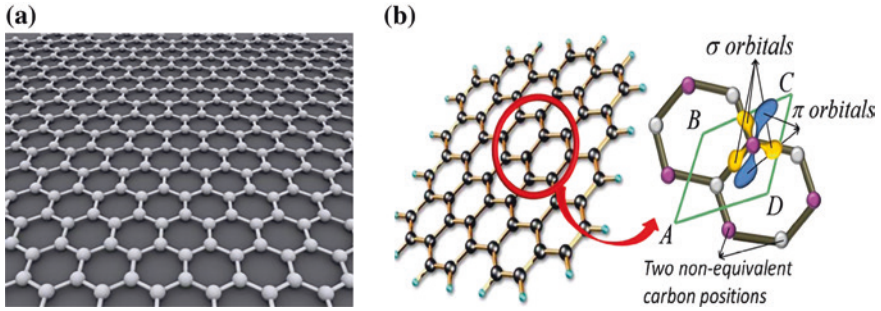


Fig. 2.1 Basic **a** hexagonal and **b** orbital structure of graphene (Reproduced with permission from Sarkar et al. 2011)

Carbon nanotubes (CNTs) are made by rolling up of sheet of graphene into a cylinder. These nanostructures are constructed with length-to-diameter ratio of up to $(1.32 \times 10^8):1$ (Wang 2009) that is significantly larger than any other material. As their name suggests, the diameter of nanotube is in the order of few nanometers, while they can be up to 18 centimeters in length (Javey and Kong, 2009). CNTs are most promising candidates in the field of nanoelectronics, especially for interconnect applications. Metallic CNTs have aroused a lot of research interest for their applicability as VLSI interconnects due to high thermal stability, high thermal conductivity, and large current carrying capability. A CNT can carry current density in excess of 10^3 MA/cm^2 , which can enhance the electrical performance as well as eliminate electromigration reliability concerns that plagues current nanoscale Cu interconnects (Wei et al., 2001). Recent modeling works have revealed that CNT bundle interconnects can potentially offer added advantages over Cu. Moreover, recent experiments have demonstrated that the resistance values as small as 200Ω can be achieved in CNT bundles.

2.2 Structure and Types of Carbon Nanotubes

To understand the crystal structure of CNTs, it is necessary to understand their atomic structure. Both CNTs and GNRs (graphene nanoribbons) can be understood as structures derived from a graphene sheet, shown in Fig. 2.2. A graphene sheet is a single layer of carbon atoms packed into 2D honeycomb lattice structure. CNT, considered as rolled-up graphene sheet, have the edges of the sheet joint together to form a seamless cylinder. The dashed arrows in Fig. 2.2a, b show the circumferential vector \vec{C} , which indicates the rolling up direction for CNT. The vector is defined as $\vec{C} = n_1 \hat{a}_1 + n_2 \hat{a}_2$ where \hat{a}_1 and \hat{a}_2 are the lattice vectors of graphene and n_1 and n_2 are the chiral indices. The chiral indices (n_1, n_2) uniquely defines the chirality, or the rolled-up direction of graphene sheet. Depending on the chiral indices (n_1, n_2) , CNTs can be classified to

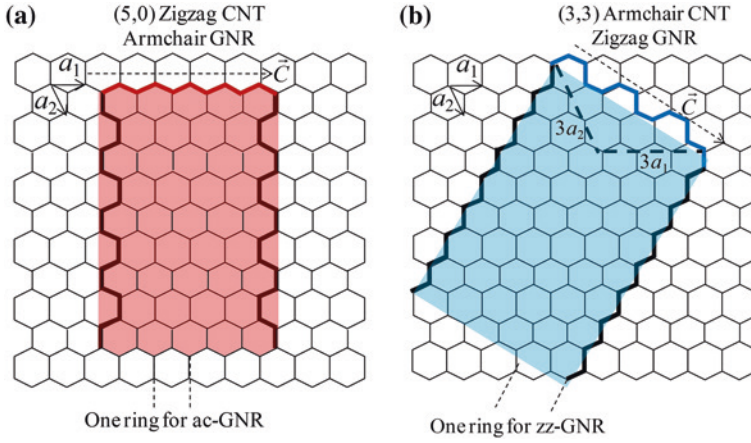


Fig. 2.2 Schematic view of CNT made from graphene sheet **a** zigzag and **b** armchair CNT

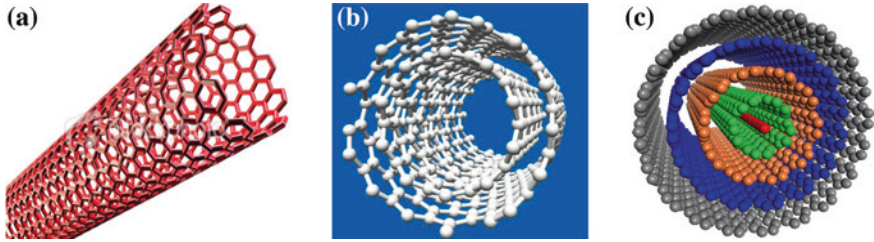


Fig. 2.3 Basic structures of **a** single-walled, **b** double-walled, and **c** multi-walled CNTs

zigzag and armchair structures as shown in Fig. 2.2a, b, respectively. For armchair CNTs, the chiral indices n_1 and n_2 are equal while for zigzag CNTs, n_1 or $n_2 = 0$ (Li et al., 2009b). For other values of indices, CNTs are known as chiral. Depending upon their different structures, CNTs can exhibit metallic or semiconducting properties. By satisfying the condition $n_1 - n_2 = 3i$ (where i is an integer), the armchair CNTs are always metallic, whereas zigzag CNTs are either metallic or semiconducting in nature (Javey and Kong 2009; Li et al. 2009b). Statistically, a natural mix of CNTs will have 1/3rd metallic and 2/3rd semiconducting chiralities.

Depending on the number of concentrically rolled-up graphene sheets, CNTs are also classified to single-walled (SWNT), double-walled (DWNT), and multi-walled CNTs (MWNT) as presented in Fig. 2.3. The structure of SWNT can be conceptualized by wrapping a one-atom-thick layer of graphene into a seamless cylinder (Majumder et al. 2011c). MWNT consists of two or more numbers of rolled-up concentric layers of graphene. DWNT is considered as a special type of MWNT wherein only two concentrically rolled up graphene sheets are present. There are two models to describe the structures of MWNT. In the Russian

Doll model, sheets of graphene are arranged in concentric cylinders, whereas, in the Parchment model (Du et al. 2005), a single sheet of graphene is wrapped around itself resembling a rolled newspaper.

2.3 Electronic Band Structure of CNTs

In order to explain the band structure of CNTs, it is essential to understand the band structure of graphene. Generally, electrical transport properties in graphene are determined by electrons and holes near the Fermi level. This is because electrons near the Fermi level have easy access to the conduction band, leaving behind the holes in the valence band. In graphene, the π orbitals are responsible for the electronic transport properties as they lie near the Fermi level. The band structure of graphene can be obtained by “tight binding approximations” method (Wallace 1947; Minto 2004; Satio et al. 1992). In Fig. 2.4a, a unit cell of graphene is shown with two non-equivalent carbon atoms A and B. With suitable combination of two unit vectors a_1 and a_2 , all other atoms can be translated back to either A or B. The reciprocal lattice of graphene with unit vectors, b_1 and b_2 is shown in Fig. 2.4b.

To obtain the band structure of graphene in π orbitals, the solutions of Schrödinger equation is required which states that

$$H\Psi = E\Psi \quad (2.1)$$

where H is the Hamiltonian, Ψ is the total wave function, and E is the energy of electrons in the π orbitals of graphene. Due to the periodic structure of graphene, the total wave function can be constructed from a linear combination of Bloch functions u_i that has a periodicity of the lattice.

In the tight binding approximation, an atomic wave function is used to represent the Bloch function u_i . The u_i for each atom can be constructed from $2p_z$ orbitals of atoms A and B as (Javey and Kong 2009)

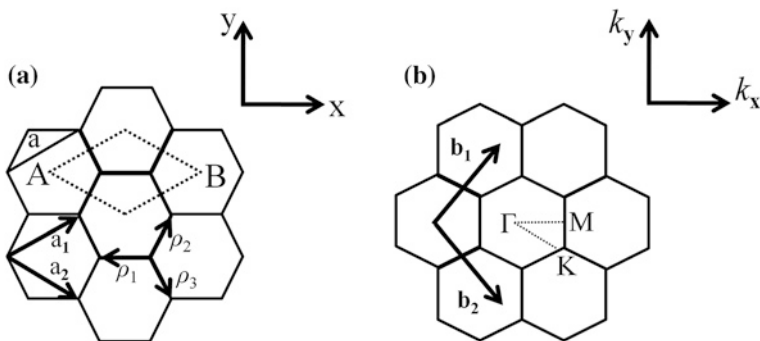


Fig. 2.4 a Real and b reciprocal space representation of a graphene lattice

$$u_{A(B)} = \frac{1}{\sqrt{N}} \sum_{A(B)} e^{ik \cdot r_{A(B)}} X(r - r_{A(B)}) \quad (2.2)$$

where $X(r)$ represents the $2p_z$ orbital wave function for an isolated carbon atom. Thus, ψ in (2.1) can be expressed as (Javey and Kong 2009)

$$\psi = C_A u_A + C_B u_B \quad (2.3)$$

Substituting Eqs. (2.3) into (2.1), the Schrödinger equation can be solved in a matrix form that can be expressed as (Javey and Kong 2009)

$$\begin{pmatrix} H_{AA} & H_{AB} \\ H_{BA} & H_{BB} \end{pmatrix} \begin{pmatrix} C_A \\ C_B \end{pmatrix} = E \begin{pmatrix} S_{AA} & S_{AB} \\ S_{BA} & S_{BB} \end{pmatrix} \begin{pmatrix} C_A \\ C_B \end{pmatrix} \quad (2.4)$$

Here,

$$H_{ij} = \langle u_i | H | u_j \rangle, \quad S_{ij} = \langle u_i | u_j \rangle \quad (2.5)$$

It is easier to neglect the overlap between $2p_z$ wave functions of different atoms, i.e., $S_{AB} = S_{BA} = 0$. For normalized case, the values can be assumed as $S_{AA} = S_{BB} = 1$; then, Eq. (2.4) is simplified to (Javey and Kong 2009)

$$\begin{pmatrix} H_{AA} - E & H_{AB} \\ H_{BA} & H_{BB} - E \end{pmatrix} \begin{pmatrix} C_A \\ C_B \end{pmatrix} = \begin{pmatrix} 0 \\ 0 \end{pmatrix} \quad (2.6)$$

The matrix Eq. (2.6) has a non-trivial solution only when

$$\begin{vmatrix} H_{AA} - E & H_{AB} \\ H_{BA} & H_{BB} - E \end{vmatrix} = 0 \quad (2.7)$$

Further, by symmetry of the graphene lattice (atoms A and B are not distinguishable), it is observed that $H_{AA} = H_{BB}$ and $H_{AB} = H_{BA}^*$. Therefore, Eq. (2.7) leads to the solution

$$E = H_{AA} \mp |H_{AB}| \quad (2.8)$$

H_{AA} ($=H_{BB}$) can be obtained by inserting Eqs. (2.2) into (2.5) as (Javey and Kong 2009)

$$H_{AA} = \frac{1}{N} \sum \sum_{A^*} e^{ik \cdot (r_A - r_A^*)} \int X^*(r - r_A) H X(r - r_A^*) d\tau \quad (2.9)$$

If the effects of the nearest neighbors are considered, the Eq. (2.9) for each atom A(B) with three nearest neighbor B(A) atoms can be obtained as (Javey and Kong 2009)

$$H_{AA} = \int X^*(r - r_A) H X(r - r_A^*) d\tau = E_0 \quad (2.10)$$

while

$$\begin{aligned} H_{AB} &= \frac{1}{N} \sum_A \sum_B e^{ik \cdot (r_A - r_B)} \int X^*(r - r_A) H X(r - r_A^*) d\tau \\ &= \frac{1}{N} \sum_i e^{ik \cdot \rho_i} \int X^*(r) H X(r - \rho_i) d\tau \end{aligned} \quad (2.11)$$

where ρ_i is a vector connecting atom A to its three nearest neighbor B atoms (as in Fig. 2.4a). By referring to the coordinate system of the graphene in Fig. 2.4a, the following expression can be obtained (Javey and Kong 2009)

$$\begin{aligned} H_{AB} &= \left(e^{ik \cdot \rho_1} + e^{ik \cdot \rho_2} + e^{ik \cdot \rho_3} \right) \int X^*(r) H X(r - \rho_1) d\tau \\ &= \gamma_0 \left(e^{-ik_x a / \sqrt{3}} + 2e^{ik_x a / 2\sqrt{3}} \cos\left(\frac{k_y a}{2}\right) \right) \end{aligned} \quad (2.12)$$

γ_0 represents the strength of exchange interaction between nearest neighbor atoms that is known as the tight-binding integral or transfer integral. Therefore, from Eqs. (2.10) and (2.12), the energy dispersion in Eq. (2.8) can be obtained as (Javey and Kong 2009)

$$E = E_0 \mp \gamma_0 \left(1 + 4 \cos\left(\frac{\sqrt{3}k_x a}{2}\right) \cos\left(\frac{k_y a}{2}\right) + 4 \cos^2\left(\frac{k_y a}{2}\right) \right)^{1/2} \quad (2.13)$$

In Eq. (2.13), negative sign represents the valence band of graphene produced by bonding π orbitals, while positive sign denotes conduction band formed by anti-bonding π^* orbitals. The dispersion relation in Eq. (2.13) is plotted in Fig. 2.5 along high-symmetry points in the reciprocal space with $E_0 = 0$. Figure 2.6a, b represent the surface and contour plots of the energy dispersion, respectively. The six K points at the corners of the Brillouin zone are the main feature of the energy dispersion of graphene. At these points, the conduction and valence bands meet resulting in zero bandgap in graphene. It can also be noted that the two K points (K_1 and K_2) are non-equivalent due to symmetry. The circular contour around each K point in Fig. 2.6b indicates the conic shape of dispersion near each K point.

2.3.1 Band Structure of CNTs from Graphene

CNTs can be uniquely defined by chiral vector, $C = n_1 a_1 + n_2 a_2$, where n_1 and n_2 are integers and a_1 and a_2 are unit vectors of the graphene lattice as shown in Fig. 2.7.

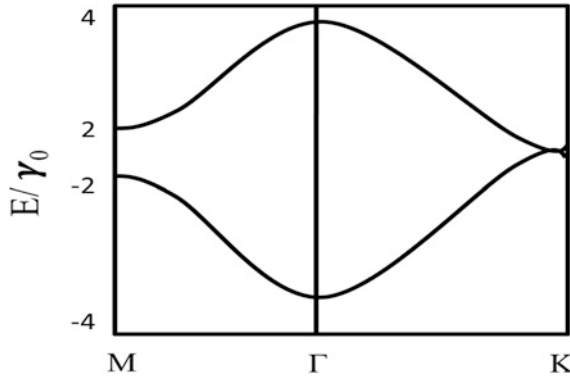


Fig. 2.5 Energy dispersion of graphene along high-symmetry points as indicated in Fig. 2.4b

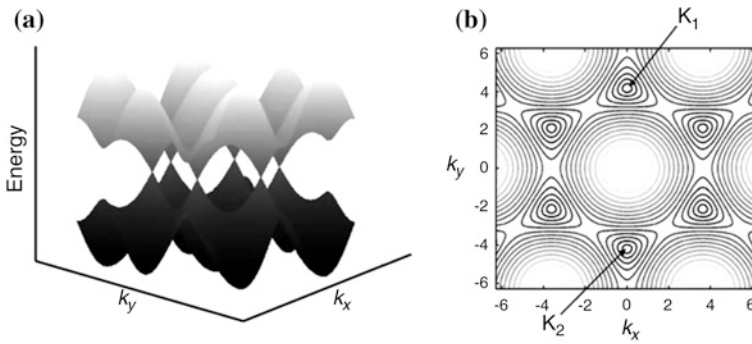


Fig. 2.6 **a** Surface plot and **b** contour plot of the energy dispersion in graphene as given by Eq. (2.13). Note that there are six K points where the bandgap becomes zero. Among the six K points, only two are non-equivalent, denoted by K_1 and K_2 (Reproduced with permission from Javey and Kong 2009)

A graphene sheet is rolled up to form CNT in such a way that two carbon atoms coincide. With wrapping indices n_1 and n_2 , CNTs can be uniquely defined and described.

Since CNT is a rolled-up sheet of graphene, an appropriate boundary condition is required to explore the band structure. If CNT can be considered as an infinitely long cylinder, there are two wave vectors associated with it: (1) the wave vector parallel to CNT axis k_{\parallel} that is continuous in nature due to the infinitely long length of CNTs and (2) the perpendicular wave vector k_{\perp} that is along the circumference of CNT. These two wave vectors must satisfy a periodic boundary condition (i.e., the wave function repeats itself as it rotates 2π around a CNT) (Javey and Kong 2009)

$$k_{\perp} \cdot C = \pi D k_{\perp} = 2\pi m \quad (2.14)$$

where D represents the diameter of CNT and m is an integer. The quantized values of allowed k_{\perp} for CNTs are obtained from the boundary condition.

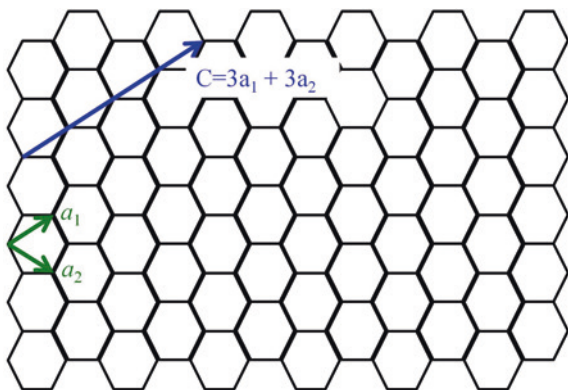


Fig. 2.7 Representation of CNT (single-walled) by a chiral vector, $C = n_1 a_1 + n_2 a_2$

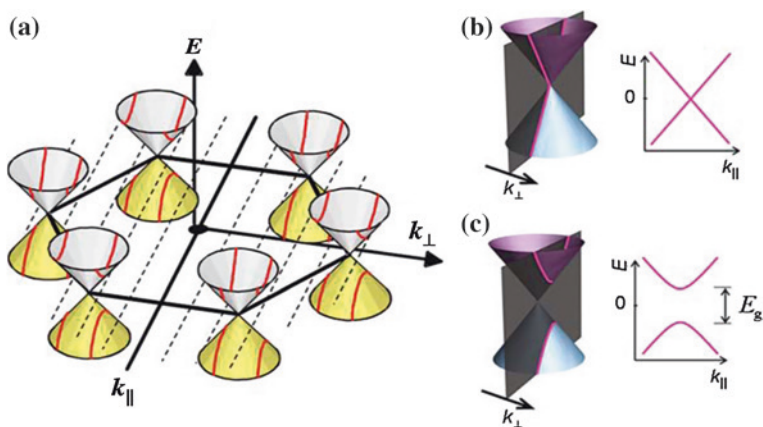


Fig. 2.8 **a** A first Brillouin zone of graphene with conic energy dispersions at six K points. The allowed k_{\perp} states in CNT are presented by *dashed lines*. The band structure of CNT is obtained by cross sections as indicated. Zoom-ups of the energy dispersion near one of the K points are schematically shown along with the cross sections by allowed k_{\perp} states and resulting 1D energy dispersions for **b** a metallic CNT and **c** a semiconducting CNT (Reproduced with permission from Javey and Kong 2009)

The cross-sectional cutting of the energy dispersion with the allowed k_{\perp} states results in 1D band structure of graphene as shown in Fig. 2.8a. This is called zone folding scheme of obtaining the band structure of CNTs. Each cross-sectional cutting gives rise to 1D subband. The spacing between allowed k_{\perp} states and their angles with respect to the surface Brillouin zone determine the 1D band structures of CNTs. The band structure near the Fermi level is given by allowed k_{\perp} states that are closest to the K points. When the allowed k_{\perp} states pass directly through the K points as shown in Fig. 2.8b, the energy dispersion has two linear bands crossing at the Fermi level without a bandgap. However, if the allowed k_{\perp}

states miss the K points as shown in Fig. 2.8c, there are two parabolic 1D bands with an energy bandgap. Therefore, two different kinds of CNTs can be expected depending on the wrapping indices, firstly, the metallic CNTs without bandgap as in Fig. 2.8b, and secondly, the semiconducting CNTs with bandgap as in Fig. 2.8c.

2.3.2 Metallicity and Semiconducting Properties of Zigzag CNTs

Using the approach of 1D subbands discussed in previous subsection, the 1D subband closest to the K points for zigzag CNTs is investigated here. The zigzag CNTs can be either metallic or semiconducting depending on their chiral indices. Since the circumference is na ($C = na_1$), the boundary condition in Eq. (2.14) becomes (Javey and Kong 2009)

$$k_x na = 2\pi m \quad (2.15)$$

There is an allowed k_x that coincides with K point at $(0, 4\pi/3a)$. This condition arises when n has a value in multiple of 3 ($n = 3q$, where q is an integer). Therefore, by substitution in Eq. (2.15) (Javey and Kong 2009)

$$k_x = \frac{2\pi m}{na} = \frac{3Km}{2n} = \frac{Km}{2q} \quad (2.16)$$

There is always an integer m ($=2q$) that makes k_x pass through K points so that these kinds of CNTs (with $n = 3q$) are always metallic without bandgap as shown in Fig. 2.8b. There are two cases when n is not a multiple of 3. If $n = 3q + 1$, the k_x is closest to the K point at $m = 2q + 1$ (as in Fig. 2.8c).

$$k_x = \frac{2\pi m}{na} = \frac{3Km}{2n} = \frac{3K(2q+1)}{2(3q+1)} = k + \frac{K}{2} \frac{1}{3q+1} \quad (2.17)$$

Similarly, for $n = 3q - 1$, the allowed k_x closest to K is when $m = 2q - 1$; hence (Javey and Kong 2009)

$$k_x = \frac{2\pi m}{na} = \frac{3Km}{2n} = \frac{3K(2q-1)}{2(3q-1)} = k - \frac{K}{2} \frac{1}{3q-1} \quad (2.18)$$

In these two cases, allowed k_x misses the K point by (Javey and Kong 2009)

$$\Delta k_x = \frac{K}{2} \frac{1}{3q \pm 1} = \frac{2}{3} \frac{\pi}{na} = \frac{2}{3} \frac{\pi}{\pi D} = \frac{2}{3D} \quad (2.19)$$

From Eq. (2.19), it is inferred that the smallest misalignment between an allowed k_x and a K point is inversely proportional to the diameter. Thus, from the slope of a cone near K points (Eq. 2.14), the bandgap E_g can be expressed as

$$E_g = 2 \times \left(\frac{\partial E}{\partial k} \right) \times \frac{2}{3D} = 2\hbar v_F \left(\frac{2}{3D} \right) \approx 0.7\text{eV}/D \text{ (nm)} \quad (2.20)$$

Therefore, semiconducting CNTs ($D = 0.8\text{--}3\text{ nm}$) exhibit bandgap ranging from 0.2 to 0.9 eV. Depending on the different values of p , three different conditions can be occurred that describes the metallicity and semiconducting properties of CNTs (Javey and Kong 2009):

- (a) $p = 0$; metallic with linear subbands crossing at the K points.
- (b) $p = 1, 2$; semiconducting with a bandgap, $E_g \sim 0.7\text{ eV}/D\text{ (nm)}$.

Similar treatment can also be applied for armchair CNTs (n, n), arriving at the conclusion that they are always metallic.

2.4 Properties of CNTs

The atomic arrangements of carbon atoms are responsible for the unique electrical, thermal, and mechanical properties of CNTs. These properties are discussed below:

2.4.1 Electrical Conductivity

A metallic CNT can be considered as highly conductive material. Chirality, the degree of twist of graphene sheet, determines the conductivity of CNT interconnects. Depending on the chiral indices, CNTs exhibit both metallic or semiconducting properties. The electrical conductivity of MWNTs is quite complex as their inter-wall interactions non-uniformly distribute the current over individual tubes. However, an uniform distribution of current is observed across different parts of metallic SWNT (Shah et al. 2013). Electrodes are placed to measure the conductivity and resistivity of different parts of SWNT rope. The measured resistivity of the SWNT ropes is in the order of $10^{-4}\text{ }\Omega\text{ cm}$ at $27\text{ }^\circ\text{C}$, indicating SWNT ropes to be the most conductive carbon fibers (Dresselhaus et al. 2001). It has been reported that an individual SWNT may contain defects that allows the SWNT to behave as a transistor.

2.4.2 Strength and Elasticity

Each carbon atom in a single sheet of graphite is connected via strong chemical bond to three neighboring atoms. Thus, CNTs can exhibit the strongest basal plane elastic modulus and hence are expected to be an ultimate high strength fiber. The elastic modulus of SWNTs is much higher than steel that makes them highly resistant. Although pressing on the tip of nanotube will cause it to bend, the nanotube returns to its original state as soon as the force is removed. This property makes CNTs extremely useful as probe tips for high resolution scanning probe microscopy.

Although, the current Young's modulus of SWNT is about 1 TPa, but a much higher value of 1.8 TPa has also been reported (Hsieh et al. 2006). For different experimental measurement techniques, the values of Young's modulus vary in the range of 1.22 TPa–1.26 TPa depending on the size and chirality of the SWNTs (Dresselhaus et al. 2001). It has been observed that the elastic modulus of MWNTs is not strongly dependent on the diameter. Primarily, the moduli of MWNTs are correlated to the amount of disorder in the nanotube walls (Forro et al. 2002).

2.4.3 Thermal Conductivity and Expansion

CNTs can exhibit superconductivity below 20 K (approximately -253°C) due to the strong in-plane C–C bonds of graphene. The strong C–C bond provides the exceptional strength and stiffness against axial strains. Moreover, the larger inter-plane and zero in-plane thermal expansion of SWNTs results in high flexibility against non-axial strains.

Due to their high thermal conductivity and large in-plane expansion, CNTs exhibit exciting prospects in nanoscale molecular electronics, sensing and actuating devices, reinforcing additive fibers in functional composite materials, etc. Recent experimental measurements suggest that the CNT embedded matrices are stronger in comparison to bare polymer matrices (Wei et al. 2002). Therefore, it is expected that the nanotube may also significantly improve the thermo-mechanical and the thermal properties of the composite materials.

2.4.4 Field Emission

Under the application of strong electric field, tunneling of electrons from metal tip to vacuum results in field emission phenomenon. Field emission results from the high aspect ratio and small diameter of CNTs. The field emitters are suitable for the application in flat-panel displays. For MWNTs, the field emission properties occur due to the emission of electrons and light. Without applied potential, the luminescence and light emission occurs through the electron field emission and visible part of the spectrum, respectively.

2.4.5 Aspect Ratio

One of the exciting properties of CNTs is the high aspect ratio, inferring that a lower CNT load is required compared to other conductive additives to achieve similar electrical conductivity. The high aspect ratio of CNTs possesses unique electrical conductivity in comparison to the conventional additive materials such as chopped carbon fiber, carbon black, or stainless steel fiber.

2.4.6 Absorbent

Carbon nanotubes and CNT composites have been emerging as perspective absorbing materials due to their light weight, larger flexibility, high mechanical strength and superior electrical properties. Therefore, CNTs emerge out as ideal candidate for use in gas, air and water filtration. The absorption frequency range of SWNT-polyurethane composites broaden from 6.4–8.2 (1.8 GHz) to 7.5–10.1 (2.6 GHz) and to 12.0–15.1 GHz (3.1 GHz) (Wang et al. 2013). A lot of research has already been carried out for replacing the activated charcoal with CNTs for certain ultrahigh purity applications.

2.5 Production of CNTs

A number of methods are used to produce CNTs and fullerenes. In earlier days, fullerenes were produced by vaporizing graphite with a short-pulse, high-power laser method, whereas carbon combustion and vapor deposition processes were used to produce CNTs. Using the earlier method (plasma arcing) of producing CNTs and fullerenes in reasonable quantities, an electric current was applied across two carbonaceous electrodes in an inert gas atmosphere. The plasma arcing method is primarily used to produce fullerenes and CNTs from different carbonaceous materials such as graphite. The CNTs are deposited on the electrode, while the fullerenes appear in the soot. Plasma arcing method can also be applied in the presence of cobalt with 3 % or greater concentration. Different methods for production of CNTs and fullerenes are discussed below:

2.5.1 Arc Discharge Method

The most common and easiest way to produce CNTs is the carbon arc discharge method. Using this method, a complex mixture of components is produced that separates the CNTs from soot and the catalytic metals. Arc vaporization is used to produce CNTs by placing two carbon rods from end to end, separated by an approximate distance of 1 mm, placed in an enclosure. At low pressure, the enclosure is usually filled with inert gas. A high temperature discharge between two electrodes is created by applying a direct current of 50 to 100 A. The surface of the carbon electrodes is vaporized by the high temperature discharge and finally forms a small rod-shaped electrode. The production of CNTs in high yield primarily depends on the uniformity of the plasma arc. The arc discharge method with liquid nitrogen can also be used to produce CNTs.

2.5.2 Laser Method

In 1996, a dual-pulsed laser was used in synthesization techniques for producing CNTs with 70 % purity. Presently the laser vaporization process is used for producing CNTs. In this process, a graphite rod with 50:50 catalyst mixtures of cobalt and nickel at 1200 °C in flowing argon is used to prepare the sample (Ahmed 2010). The uniform vaporization of the target can be achieved by using the initial laser vaporization pulse followed by a second pulse. The amount of deposition of carbon as soot is primarily minimized by the usage of these two successive laser pulses. The larger particles are broken by applying the second laser pulse. The CNTs produced through this process are 10–20 nm in diameter and 100 μm or more in length. The average nanotube diameter and size distribution can vary for different growth temperature, catalyst composition, and other process parameters. In recent years, the arc discharge and laser vaporization methods are used to obtain high quality CNTs in small quantity. However, both methods suffer from the following two drawbacks: (1) The methods use the evaporation of carbon source that follows an unclear approach to scale up the production with industrial standard and (2) the CNTs produced by vaporization method get mixed with residues of carbon. Therefore, it is quite difficult to purify, manipulate, and assemble CNTs for building nanotube device architectures for practical applications.

2.5.3 Chemical Vapor Deposition

From last twenty years, carbon fibers and filaments are produced using chemical vapor deposition of hydrocarbons along with a metal catalyst. In this process, large amount of CNTs is produced by catalytic CVD of acetylene over cobalt and iron. Using the carbon/zeolite catalyst, fullerenes and bundles of SWNTs can be produced along with the MWNTs. Lot of research works have been carried out for the formation of SWNTs/MWNTs from ethylene that is supported by the catalysts such as iron, cobalt, and nickel. The recent research works have also demonstrated the production of SWNTs and DWNTs on molybdenum and molybdenum–iron alloy catalysts. A thin alumina template with or without nickel catalyst is achieved using the CVD of carbon within the pores. Ethylene can be used with reaction temperatures of 545 °C for Nickel-catalyzed CVD and 900 °C for an uncatalyzed process that produces carbon nanostructures with open ends (Che et al. 1998). Methane can also be used as carbon source for synthesization. Catalytic decomposition of H_2/CH_4 mixture over cobalt, nickel, and iron is used to obtain high yields of SWNTs at 1,000 °C. The usage of H_2/CH_4 atmosphere between a non-reducible oxide such as Al_2O_3 or MgAl_2O_4 and one or more transition metal oxides can produce the composite powders containing well-dispersed CNTs. Thus, higher proportions of SWNTs and lower proportions of MWNTs can be achieved using the decomposition of CH_4 over the freshly formed nanoparticles.

2.5.4 Ball Milling

One of the simple methods for the production of CNTs is through ball milling followed by subsequent annealing. Thermal annealing is used to produce CNTs from carbon and boron nitride powder. In this method, graphite powder is placed in a stainless steel container consisting of four hardened steel balls. The steel container is purged, and argon is introduced for milling process, at room temperature, for up to 150 h (Wilson et al. 2002). Using the milling process, the annealing of graphite powder is carried out under an inert gas flow at 1400 °C for 6 h. This method produces more MWNTs and few SWNTs.

2.5.5 Other Methods

Apart from the above mentioned synthesis methods, CNTs can also be produced using electrolysis, flame synthesis, synthesis from bulk polymer, use of solar energy and low-temperature solid pyrolysis. Using the electrolysis method, CNTs are produced by passing an electric current in molten ionic salt between graphite electrodes. High-purity carbon rod is used as cathode. At high melting point, the cathode is consumed and a wide range of nanomaterials are produced. In the flame synthesis method, a portion of the hydrocarbon gas is provided at an elevated temperature that is required for the hydrocarbon reagents to function. The CNTs can also be synthesized chemically by using polymers consisting of carbon. This process can produce MWNTs with diameters ranging from 5 nm to 20 nm and a length upto 1 μm (Journet and Bernier, 1998).

Several research groups (Chibante et al. 1993; Laplaze et al. 1996) demonstrated the production of fullerenes using highly concentrated sunlight from a solar furnace. Using this method, sunlight is focused on a graphite sample to condense the carbon soot in a cold dark zone of the reactor. The pyrolysis method is used to synthesize CNTs from metastable carbon containing compounds at relatively low temperature of 1200 °C to 1900 °C. This method produces MWNTs of diameters ranging from 10 nm to 25 nm and lengths of 0.1–1 μm .

2.6 Purification of CNTs

After synthesization, purification of CNTs is done by separating it from other entities, such as amorphous carbon, carbon nanoparticles, residual catalyst and other unwanted species. The classic chemical techniques are proved as ineffective for removing the undesirable impurities from CNTs. Therefore, three basic methodologies such as gas phase, liquid phase, and intercalation are used to purify the CNTs from the undesirable impurities.

Generally, a microfiltration operation is performed to remove the nanoparticles using membrane filters. This methodology removes the amorphous carbon and unwanted nanoparticles simultaneously without chemically modifying the CNTs.

Furthermore, the smaller chemical substances can be removed by applying only 2–3 mol. nitric acid (Wilson et al. 2002). Using the extended sonication in concentrated acid mixtures, CNTs are cut into smaller segments, forming colloidal suspension in solvents. The solvents can be deposited on substrates or in solution that provides different functional groups attached to the ends and sides of the CNTs. The details of different purification methods are discussed below:

2.6.1 Gas Phase

Thomas Ebbesen and his coworkers developed the most successful technique for purification of nanotubes that is formally known as gas-phase method (Ebbesen 1996). Using this method, the researchers realized that the oxidization process is easier for the nanoparticles with defect as compared to the relatively perfect nanotubes. This method produces significant enrichment of nanotubes.

Recently, NASA Glenn Research Center introduced a new gas-phase method for purification of SWNTs in gram-scale quantities (Glenn Research Center 2002). This purification method uses the combination of high temperature oxidation and repeated extraction with nitric and hydrochloric acid. Using this improved procedure, the stability of the nanotube is significantly improved with a negligible reduction of impurities such as residual catalyst and non-nanotube forms of carbon.

2.6.2 Liquid Phase

Another effective purification method is the liquid-phase methodology. The current liquid-phase purification method follows the essential steps described below:

- Preliminary filtration—used to remove large graphite particles
- Dissolution—used to remove fullerenes and catalyst particles
- Microfiltration
- Centrifugal separation and
- Chromatography

In this process, CNTs are subjected to the liquid phase oxidation step with hydrogen peroxide (H_2O_2) solution. It removes the amorphous carbon without damaging the tube walls. Thus, it becomes quite easy to separate CNTs in the last stage of separation.

2.6.3 Intercalation

Intercalation technique is used to insert a molecule (or ion) into compounds with layered structures. This technique expands the Vander Waals gap between adjacent layers, which requires energy. This energy is usually supplied by the charge transfer between the dopants and the solid.

A research group introduced the intercalation methodology with a variety of materials to purify the nanotubes (Harris 1999). Using the intercalation with Cu chloride, it is preferentially easy to oxidize the nanoparticles away. Thus, this process became popular for purification of nanotubes. In the first stage, the cathode is immersed in a molten copper chloride and potassium chloride mixture for one week at 400 °C. To remove the excess copper chloride and potassium chloride, ion exchanged water is used to wash the mixture of graphitic fragments and the intercalated nanoparticles. The washed product is slowly heated at 500 °C in a mixture of helium and hydrogen for one hour to reduce the intercalated copper chloride and potassium chloride metal. Finally, the oxidation of the material is carried out, in flowing air, at a rate of 10 °C/min to a temperature of 555 °C. This process provides a fresh sample of cathodic soot that can be treated as fresh nanotube. The drawbacks of this method are: (1) losing of some amount of nanotubes at oxidation stage and (2) contamination of the final material with residues of intercalates.

2.7 Application of CNTs

CNTs have not only unique atomic arrangements but also have unique properties (Li et al. 2009a) that include large current carrying capability (Wei et al. 2001), long ballistic transport length (Javey and Kong 2009), high thermal conductivity (Collins et al. 2001a), and mechanical strength (Berber et al. 2000). These extraordinary properties of CNTs qualifies them exciting prospects and variety of applications in the area of microelectronics/nanoelectronics (Avarious et al. 2007), spintronics (Tsukagoshi et al. 1999), optics (Misewich et al. 2003), material science (Wang et al. 2000), mechanical (Yu et al. 2000), and biological fields (Yu et al. 2000; Lu et al. 2009). Particularly, in the area of nanoelectronics, CNTs and graphene nanoribbons (GNRs) demonstrates wide range of applications such as energy storage [supercapacitor (Du et al. 2005)] devices; energy conversion devices that includes thermoelectric (Wei et al. 2009) and photovoltaic (Ago et al. 1999) devices; field emission displays and radiation sources (Choi et al. 1999); nanometer semiconductor transistors (Collins et al. 2001a), nanoelectromechanical systems (NEMS) (Dadgour et al. 2008), electrostatic discharge (ESD) protection (*Hyperion Catalysis*), interconnects (Kreupl et al. 2002; Li et al. 2009a), and passives (Li and Banerjee 2008a). The applications of CNTs in different fields are listed below.

2.7.1 Structural

CNTs possesses remarkable properties and qualities as structural materials. Their potential applications include (Jorio et al. 2008):

- (a) *Textiles*—CNTs can produce waterproof and tear-resistant fabrics.
- (b) *Body armor*—CNT fibers are being used as combat jackets. The jackets are used to monitor the condition of the wearer and to provide protection from bullets.

- (c) *Concrete*—CNTs in concrete increases its tensile strength and halt crack propagation.
- (d) *Polyethylene*—CNT fibers can be used as polyethylene. The CNT based polyethylene can increase the elastic modulus of the polymers by 30 %.
- (e) *Sports equipment*—Golf balls, golf clubs, stronger and lighter tennis rackets, bicycle parts, and baseball bats.
- (f) *Bridges*—CNTs may be able to replace steel in suspension and bridges.
- (g) *Flywheels*—The high strength/weight ratios of CNTs enable very high rotational speeds.
- (h) *Fire protection*—Thin layers of buckypaper can potentially protect the object from fire. The dense, compact layer of CNT or carbon fibers in the form of buckypaper can efficiently reflect the heat.

2.7.2 Electromagnetic

CNTs can be fabricated as electrical conductors, semiconductors and insulators. Such applications include:

- (a) *Buckypaper*—Thin nanotube sheets are 250 times stronger and 10 times lighter than steel. They can be used as heat sink for chipboards, backlight for LCD screens, or Faraday cage to protect electrical devices/aeroplanes (Ji et al. 2006). A fabricated device composed of *p*-type and *n*-type elements is shown in Fig. 2.9 (Hu et al. 2010).
- (b) *Light bulb filament*—CNTs can be used as alternative to tungsten filaments in incandescent lamps (Jornet and Akyildiz 2010).
- (c) *Magnets*—A strong magnetic field can be generated using multi-walled CNTs coated with magnetite (Jornet and Akyildiz 2010).
- (d) *Solar cells*—Germanium CNT diode exploits the photovoltaic effect. In some solar cells, nanotubes are used to replace the ITO (indium tin-oxide) to allow the light to pass to the active layers and generate photocurrent (Laplazeb et al. 1997).
- (e) *Electromagnetic antenna*—CNTs can act as an antenna for radio and other electromagnetic devices due to its durability, light weight and conductive properties (Jornet and Akyildiz 2010). The skin effect in CNTs is negligible at high frequencies due to additional kinetic inductance. This results in low power dissipation, resulting in high antenna efficiency (Huang et al. 2008).

2.7.3 Electroacoustic

The application of CNT in the field of electroacoustic is:

Loudspeaker—Loudspeakers can be manufactured from sheets of parallel CNTs. Such a loudspeaker can generate sound similar to the sound of lightening producing thunder (Jorio et al. 2008; Avouris et al. 2003, 2007).

Fig. 2.9 A fabricated demo-device composed of 50 pairs of *p*-type and *n*-type elements (Reproduced with permission from Hu et al. 2010)

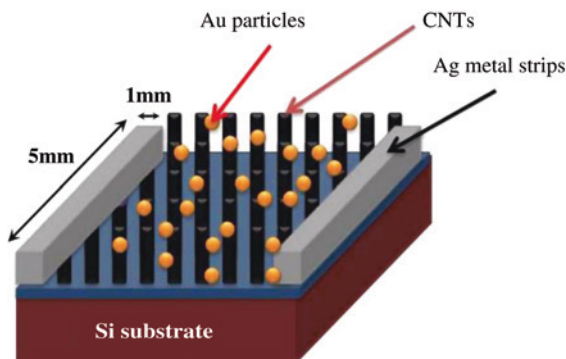


2.7.4 Chemical

CNTs finds tremendous applications in the chemical field also, few of them are as follows:

- (a) *Air pollution filter*—CNTs are one of the best materials for air filters because they possess high adsorption capacity and large specific area. The conductance of CNTs changes when polluted gas comes in its contact. This helps in detecting and filtering the polluted air (Ong et al. 2010). CNT membranes can successfully filter carbon dioxide from power plant emissions (Lin et al. 2008).
- (b) *Water filter*—CNT membranes can aid in filtration. It can reduce distillation costs by 75 %. These tubes are so thin that small particles (like water molecules) can pass through them, while blocking larger particles (such as the chloride ions in salt) (Jorio et al. 2008; Lin et al. 2008).
CNTs have high active site and controlled distribution of pore size on their surface. This increases not only its sorption capabilities, but also its sorption efficiency. CNTs have effective sorption capacity over broad pH range (particularly for 7 to 10 pH) (Ong et al. 2010).
- (c) *Chemical Nanowires*—The CNTs finds their applications in nanowire manufacturing using materials such as gold, zinc oxide, gallium arsenide, etc. The gold based CNT nanowires are very selective and sensitive to hydrogen sulphide (H_2S) detection. The zinc oxide (ZnO) based CNT nanowires can be used in applications for light emitting devices and harvesters of vibrational energy (Ok et al. 2010).
- (d) *Sensors*—CNT based sensors can detect temperature, air pressure, chemical gases (such as carbon monoxide, ammonia), molecular pressure, strain, etc. The operation of a CNT based sensor is primarily dependent on the generation of current/voltage. The electric current is generated by the flow of free charged carrier induced in any material. This charge is typically modulated by the adsorption of a target on the CNT surface (Martin et al. 2012). A CNT based fabricated gas sensing device is shown in Fig. 2.10 (Lin et al. 2013).

Fig. 2.10 Fabricated gas sensing device (Reproduced with permission from Lin et al. 2013)



2.7.5 Mechanical

The potential application of CNTs can be found in the following areas of mechanical engineering as well :

- (a) *Oscillator*—Oscillators based on CNTs have achieved higher speeds than other technologies (>50 GHz) (Jorio et al. 2008). Researchers reported a molecular oscillator with frequencies upto several gigahertz. The operation of this oscillator is primarily based on the low friction and low wear bearing properties of a multi-walled CNT with a diameter ranging from 1 nm to a few tens of nanometers.
- (b) *Waterproof*—CNTs can be used to prepare superhydrophobic cotton fabric by dip-coating approach. This approach is solely based on the chemical reactions caused by UV-activated nitrene solution. The solution is used to transform the cotton fabric surface from hydrophilic to superhydrophobic with an apparent water contact angle of 154° . Since CNTs are covalently attached on the surface of the cotton fabric, the superhydrophobicity possesses high stability and chemical durability (Jorio et al. 2008).

2.7.6 Optical

Carbon nanotubes are grown like a field of grass, where each nanotube is separated like a blade of grass. Thus, a particle of light bounces between the nanotubes. In this process, light is completely absorbed and it is converted to heat. Therefore, the absorbance of CNT is extremely high in wide ranges from FUV to FIR (Mizuno et al. 2009) [FUV (Far Ultraviolet): 100-200 nm; FIR (Far Infrared): 50-1000 μm].

2.7.7 Electrical Circuits

CNTs are attractive materials in fundamental science and technology. They have demonstrated unique electrical properties for building electronic devices, such as CNT field-effect transistors (CNTFETs) and CNT diodes. CNTs can be used to form a p - n junction diode by chemical doping and polymer coating. These types of diodes can be used to form a computer chip. CNT diodes can potentially dissipate heat out of the computer chips due to their unique thermal transmission properties (Jorio et al. 2008).

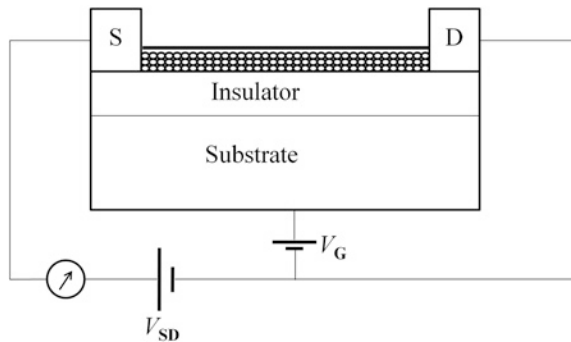
2.7.8 Interconnects

Carbon nanotubes (CNTs) have emerged as one of the most potential interconnect material solutions in current nanoscale regime. The higher current density of 1000 MA/sq-cm of an isolated CNT can eliminate the electromigration reliability concerns that plagues the current nanoscale copper interconnects. Therefore, CNT interconnects can potentially offer immense advantages over copper in terms of crosstalk, delay and power dissipation (Li et al. 2008b; Banerjee and Srivastava 2006a).

2.7.9 Transistors

CNTs can form conducting channels in transistor configurations as shown in Fig. 2.11. Two different device architectures have been developed for the transistor configuration. In both cases, CNTs connect the source and drain electrodes and show excellence behavior in the area of memory designing, amplifiers, sensors and detectors, etc. In one device architecture, the source and the drain are connected by a single nanotube. In other device architecture, a random array of nanotubes

Fig. 2.11 CNT-based transistor



functions as a conducting channel (Gruner 2005; Banerjee and Srivastava 2006a; Raychowdhury and Roy 2006; Wind et al. 2002, 2003; Hasan et al. 2006; Appenzeller et al. 2005; Manney et al. 1992). The advantages of CNTFET over Si-MOSFET are as follows (Sahoo and Mishra 2009):

- (i) CNTFET demonstrates higher drive current compared to Si-MOSFET.
- (ii) CNTFET shows approximately four times higher transconductance than Si-MOSFET.
- (iii) The average carrier velocity of CNTFET is almost double the Si-MOSFET.

This chapter presented the unique atomic structures, properties and applications of carbon nanotubes. The electrical, mechanical and thermal properties of CNTs are primarily dependent on their diameter and chirality. In addition to this, the chapter summarized different production and purification methods for SWNTs and MWNTs.

Carbon Nanotube Based VLSI Interconnects
Analysis and Design

Kaushik, B.K.; Majumder, M.K.

2015, XI, 86 p. 57 illus., Softcover

ISBN: 978-81-322-2046-6